ACS OMEGA

Open Access

http://pubs.acs.org/journal/acsodf

Article

Naphthalene *peri*-Diselenide-Based BODIPY Probe for the Detection of Hydrogen Peroxide, *tert*-Butylhydroperoxide, Hydroxyl Radical, and Peroxynitrite Ion

Babli Chhillar, Nikhil Sodhi, Rajni Kadian, Eliane Ribeiro Neres, Manisha Yadav, Manisha Kundu, Vinutha K. Venkatareddy, Rajeswara Rao Malakalapalli, Jamal Rafique,* Sumbal Saba,* and Vijay P. Singh*

Cite This: *ACS Omega* 2025, 10, 6396−6405

Read Online

ACCESS | Metrics & More | Article Recommendations | Supporting Information

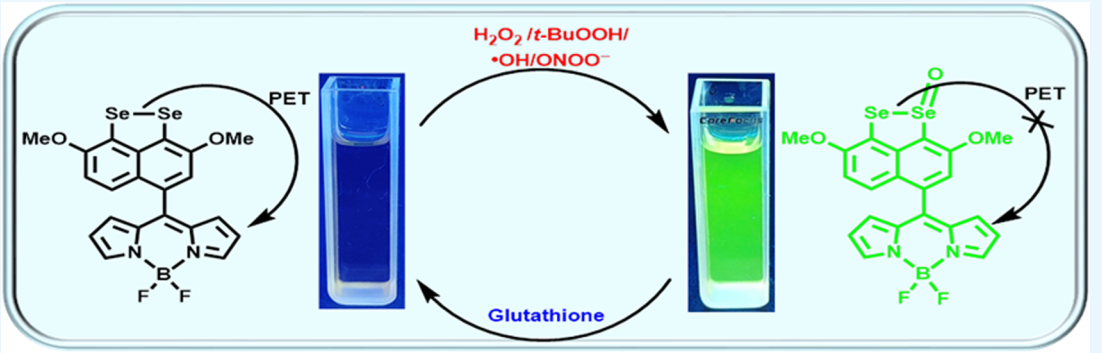

ABSTRACT: Dimethoxynaphthalene peri-diselenide-based BODIPY (4,4-difluoro-4-bora-3a,4a-diaza-s-indacene) probe has been synthesized. The probe demonstrated selectivity and sensitivity for hydrogen peroxide (H_2O_2) and *tert*-butylhydroperoxide (*t*-BuOOH), hydroxyl radical ($^{\bullet}OH$), and peroxynitrite ion ($ONOO^-$) detection and reversibility upon treatment with glutathione. The limits of detection of the probe were observed to be 0.40 μM for H_2O_2, 0.41 μM for *t*-BuOOH, 0.95 μM for $^{\bullet}OH$, and 0.46 μM for $ONOO^-$, respectively. A proposed mechanism for the "turn-on" event has been suggested and corroborated by spectroscopic and computational data. It has been proposed that electron transfer occurred from the Se center to the BODIPY moiety, followed by the photoinduced electron transfer (PET) mechanism.

INTRODUCTION

Over the last few decades, organoselenium compounds have garnered increasing interest in the field of medicine, enzymology, and bio-organic chemistry.[1] In particular, these are known to exhibit excellent biological activities including anti-inflammatory, antitumor, antifungal, and antioxidant properties.[2,3] Selenium is a key component at the active site of crucial glutathione peroxidase (GPx) enzymes.[4] In the presence of glutathione, it converts biological hydrogen peroxide (H_2O_2) into water.[5] Several organoselenium compounds have been created to replicate the activity of GPx-enzymes.[6−12] In recent years, selenium,[13,14] sulfur,[15] and tellurium-based[16,17] compounds have appeared as potential sensors for detecting metal ions, reactive nitrogen species (RNS), reactive oxygen species (ROS), and biothiols. The biological system contains ROSs such as superoxide ($O_2^{\bullet-}$), H_2O_2, *tert*-butylhydroperoxide (*t*-BuOOH), hypochlorite (^-OCl), hydroxide radical ($^{\bullet}OH$), and *tert*-butoxide (*t*-BuO$^{\bullet}$) in conjunction with RNS such as peroxynitrite ($ONOO^-$) and nitric oxide ($^{\bullet}NO$).[18] Each species plays a specific role in cellular processes including signal transduction, neurotransmission, and smooth muscle relaxation. However, the excessive production of these species can disrupt the equilibrium and lead to oxidative stress.[19] These highly reactive species are associated with various human disorders, including Alzheimer's disease, Parkinson's disease, and cancer.[20−22] Indeed, for monitoring the concentration of ROS, it is crucial to design redox-responsive fluorescent probes with good reversibility.[23] The application of fluorescence technique in identifying vital biologically important analytes has garnered enormous attention due to its exceptional sensitivity, swift response times, easy implementation, and considerable

Received: June 13, 2024
Revised: February 4, 2025
Accepted: February 7, 2025
Published: February 13, 2025

https://doi.org/10.1021/acsomega.4c05366
ACS Omega 2025, 10, 6396−6405

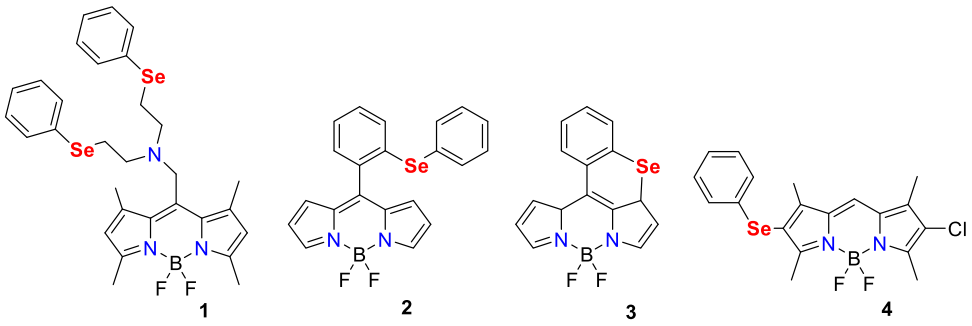

Figure 1. Reported BODIPY-based organoselenium probes **1**−**4**.

Scheme 1. Synthesis of Methoxy-Substituted Cyclic Diselenide-Containing BODIPY-Based Probe 9

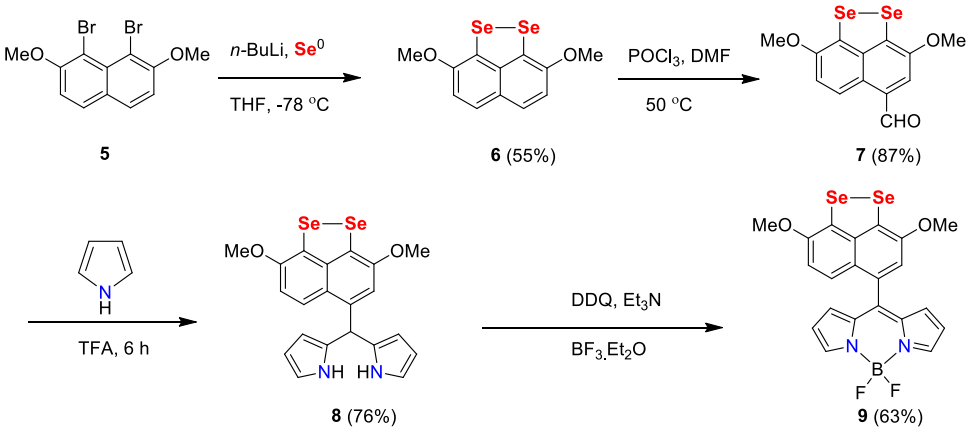

potential for imaging cells and tissues.[24,25] Many fluorescent organoselenium probes have been designed for the detection of ROS,[26] RNS,[27] and biothiols.[28] BODIPY (4,4-difluoro-4-bora-3a,4a-diaza-s-indacene) is known for its unique characteristics, such as good photochemical stability, a notable extinction coefficient, and strong fluorescence featuring a high quantum yield.[29−31]

Wu et al. prepared a novel BODIPY-based fluorescent organoselenium probe **1** via the reaction of bis[2-(phenylselenyl)ethyl]amine and 8-[chloromethyl]-4,4-difluoro-1,3,5,7-tetramethyl-4-bora-3a,4a-diaza-s-indacene under mild basic conditions in tetrahydrofuran for the detection of metal ions (Figure 1).[32]

The chelation of Cu^{2+} to the chelating groups of probe **1** increased the fluorescence of the BODIPY moiety by inhibiting photoinduced electron transfer (PET) from the Se center to the BODIPY moiety. Another BODIPY-based organoselenium probe **2** was obtained from the oxidation of 2-(phenylselenyl)-phenyldipyrromethane with 2,3-dichloro-5,6-dicyano-1,4-benzoquinone (DDQ) subsequently followed by the incorporation of borontrifluoride diethyl etherate ($BF_3{\cdot}Et_2O$). Probe **2** has shown an intensified fluorescence due to the construction of selenoxide upon the addition of HOCl.[33] Later, Churchill and co-workers reported a BODIPY-based probe **3**, synthesized from the reaction of bis(*o*-formylphenyl)diselenide with DDQ, $BF_3{\cdot}Et_2O$, and triethylamine (Et_3N),[34] showing a selective detection of $^{-}$OCl and remarkably quick response with high sensitivity, exhibiting a strong red fluorescence. The observed fluorescence enhancement was attributed to the inhibition of PET from the phenyl selenide group to the BODIPY moiety. The same group has also synthesized a novel "turn-on" phenyl selenide BODIPY-based probe **4** by the reaction of monochlorinated BODIPY compound with phenylselenyl chloride. Probe **4** exhibits high sensitivity and selectivity for $^{-}$OCl.[35] Upon the addition of HOCl, probe **4** displayed remarkable fluorescent enhancement by terminating the PET process. Further, Manjare and co-workers developed a Se-containing diBODIPY-based fluorescence probe.[36] In the presence of $O_2^{\bullet-}$, the probe showed "turn-on" event due to the quenching of the PET process. Subsequently, a cyclic diselenide-containing BODIPY probe was developed for the sensitive and selective detection of $O_2^{\bullet-}$.[37]

Organoselenium compounds, when used as small molecular probes for the biosensing of ROSs, allow for the observation of biochemical and biomolecular processes within organisms at the cellular level. Also, organoselenium compounds have a wide range of potential applications, extending from basic biological research to clinical diagnostics. Recently, various organoselenium probes have been reported. Nonetheless, as far as we are aware, there are only a few reports on selenium-based probes for the detection of H_2O_2 has been described yet.[38] Thus, in connection with our continuing interest in organoselenium compounds,[7−12] we present the synthesis of BODIPY-based molecular probe, having methoxy-substituted cyclic diselenide, used successfully for the selective detection of H_2O_2, *t*-BuOOH, $^{\bullet}$OH, and $ONOO^{-}$.

RESULTS AND DISCUSSION

Diselenide **6** was prepared by subjecting 1,8-dibromo-2,7-dimethoxynaphthalene (**5**) to lithium-halogen exchange followed by elemental Se insertion in dry THF at −78 °C (Scheme 1).[39]

Diselenide **6** was fully characterized using the spectroscopic technique, and all data were in good agreement with reported

https://doi.org/10.1021/acsomega.4c05366
ACS Omega 2025, 10, 6396−6405

values. During the purification, compound **6** crystallized via slow evaporation in open air, forming purple needle-shaped crystals. Compound **6** was then treated with phosphorus oxychloride ($POCl_3$) in dry DMF to yield *p*-formylnaphthyl diselenide **7**. Subsequently, in the presence of catalytic amount of trifluoroacetic acid (TFA), compound **7** was treated with pyrrole (4.5 equiv) under an inert atmosphere to produce dipyrrolemethane diselenide **8**. The desired BODIPY-based probe (methoxy-substituted cyclic diselenide) **9** was prepared from the reaction of compound **8** with DDQ in dichloromethane (DCM) followed by the addition of Et_3N and $BF_3{\cdot}Et_2O$. The reaction progress was checked using thin-layer chromatography (TLC), revealing a distinct new spot after each reagent addition. After completion of the reaction, the crude residue was purified by column chromatography and characterized using NMR (^1H, $^{13}C\{^1H\}$, $^{77}Se\{^1H\}$), and HRMS spectroscopic techniques. For probe **9**, in the ^1H NMR spectrum, signal for the aliphatic C−H proton disappeared. Additionally, the two signals for two chemically different Se atoms in probe **9** were shifted downfield compared with **8**, further confirming the formation of probe **9** (see Figure S11).

FTIR Analysis of Probe 9. The FTIR spectrum of probe **9** revealed several key peaks, each associated with specific functional groups (Figure S13). The peak at 3142 cm^{-1} corresponded to the C−H stretching vibration (aromatic rings). The peak at 1545 cm^{-1} is attributed to C=C stretching within the pyrrole ring, reflecting its conjugated double bond system. The 1389 cm^{-1} peak is assigned to C−O stretching in the methoxy (OMe) group, further confirmed by a secondary peak at 1256 cm^{-1}. The peak at 1057 cm^{-1} represented the stretching of the C−N bond in the ring structure. The presence of B−N stretching vibrations is indicated by the peak at 782 cm^{-1}.[40] Finally, the 581 cm^{-1} peak is associated with Se−C stretching, indicating a selenium−carbon bond.[41] This comprehensive spectral profile confirmed the successful incorporation of methoxy, pyrrole, selenium, and boron-containing groups in compound **9**.

X-ray Crystallographic Structure Analysis. Needle-shaped, purple-colored crystals of compound **6**, suitable for single-crystal X-ray diffraction analysis, were grown through slow evaporation of solvent from a solution of ethyl acetate and *n*-hexane at ambient temperature (Figure 2).

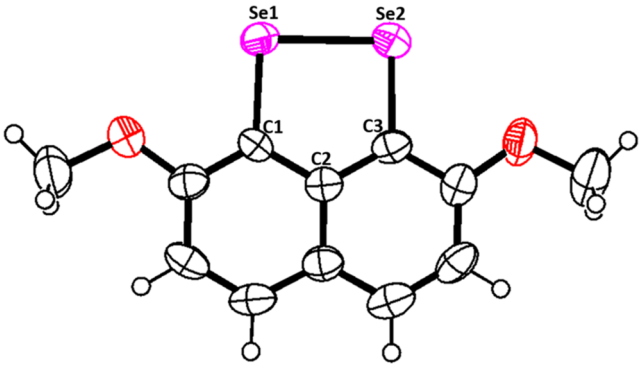

Figure 2. ORTEP view of compound **6** with a 50% probability of thermal ellipsoids. Significant bond lengths [Å] C1−Se1 1.902(6); C3−Se2 1.915(6); Se1−Se2 2.358(11) and angles [deg] C1−Se1−Se2 91.6(2); Se1−Se2−C3 90.8(2); C1−C2−C3 121.1(6); Se1−C1−C2 117.9(5); Se2−C3−C2 118.6(5).

Diselenide **6** was crystallized in monoclinic mode with space group $P2_1/n$. The C1−Se1−Se2 and Se1−Se2−C3 bond angles were found to be 90.86 and 91.65, respectively, indicating V-shaped geometry around the Se atoms.

After the successful synthesis of probe **9**, its ability to selectively and sensitively detect biologically important analytes was evaluated. First, the absorption solvatochromic studies were conducted in various solvents ranging from low-polarity hexane to high-polarity methanol, showing minimal effect (see Figure S14). The spectroscopic (UV−vis and fluorescence) properties of probe **9** with ROS were examined in a methanol/water (70:30) mixture. The 70:30 methanol/water mixture was used for the UV−vis and fluorescence studies of probe **9** to provide an optimal solvent environment that was necessary for the probe's solubility. In the initially taken 50:50 MeOH/water mixture, the probe was not completely soluble. Probe **9** was screened with various ROSs such as ^-OCl, $O_2^{\bullet-}$, H_2O_2, *t*-BuOOH, *t*-BuO$^\bullet$, and $^\bullet OH$ in water using a UV−vis spectrophotometer. The results showed an absorption maximum for probe **9** at 500 nm, with a range from 430 to 530 nm (see Figure S15). Probe **9** displayed no emission due to the electron transfer interaction between BODIPY and the selenium moiety. This, electron transfer interaction can be interrupted by the oxidation of selenium to selenoxide which is expected to result in strong emission.

Therefore, fluorescence studies were carried out for probe **9** with various ROSs/RNSs (^-OCl, $O_2^{\bullet-}$, H_2O_2, *t*-BuOOH, *t*-BuO$^\bullet$, $^\bullet OH$, and $ONOO^-$), glutathione, and ascorbic acid. Probe **9** displayed absorption at 485 nm and emission at 525 nm, exhibiting almost negligible emission intensity (Figure 3).

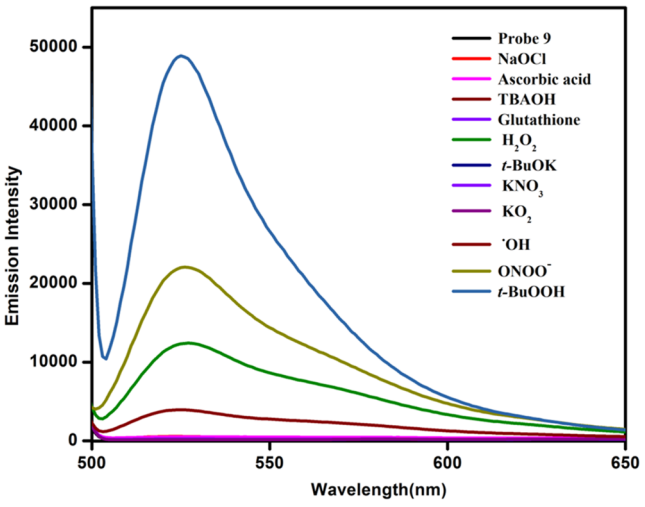

Figure 3. Emission spectra of probe **9** (10 μM, methanol/water: v/v = 70:30) with various ROSs, glutathione, and ascorbic acid (λ_{ex} = 485 nm and λ_{em} = 525 nm).

Upon addition of H_2O_2, probe **9** displayed strong yellow "turn-on" fluorescence over the other ROSs/RNSs (^-OH, ^-OCl, $O_2^{\bullet-}$, and NO_3^-) (Figure 3), glutathione, and ascorbic acid due to the oxidation of selenium to selenoxide (see Figure S16). It also showed some shift in the presence of *t*-BuOOH, $^\bullet OH$, and $ONOO^-$. However, relatively high reactivity was observed toward H_2O_2 (Figure 3).

By increasing the concentration study, a linear increase in the fluorescence intensity was noticed with a gradual increase in H_2O_2 concentrations from 0 to 400 μM (Figure 4).

https://doi.org/10.1021/acsomega.4c05366
ACS Omega 2025, 10, 6396−6405

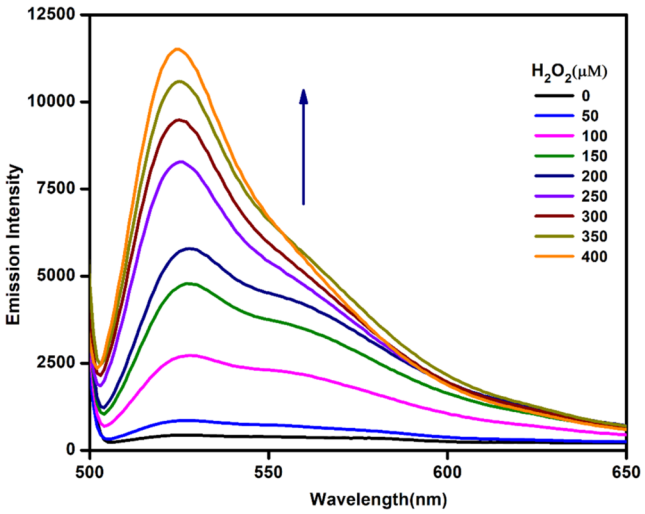

Figure 4. Emission spectra of **9** (10 μM, methanol/water: v/v = 70:30) with increasing concentrations of H_2O_2 (0−400 μM) (λ_{ex} = 485 nm and λ_{em} = 525 nm).

Probe **9** also showed a linear increase in fluorescence intensity upon a gradual increase in the concentration of *t*-BuOOH, $^{\bullet}$OH, and $ONOO^-$ (see Figures S17−S19). The limit of detection (LOD) of the probe was established by plotting the intensity against concentrations of H_2O_2, *t*-BuOOH, $^{\bullet}$OH, and $ONOO^-$ (Figures 5 and S20−S22, respectively). The LOD values of probe **9** were found to be 0.40 μM for H_2O_2, 0.41 μM for *t*-BuOOH, 0.95 μM for $^{\bullet}$OH and 0.46 μM for $ONOO^-$, respectively.

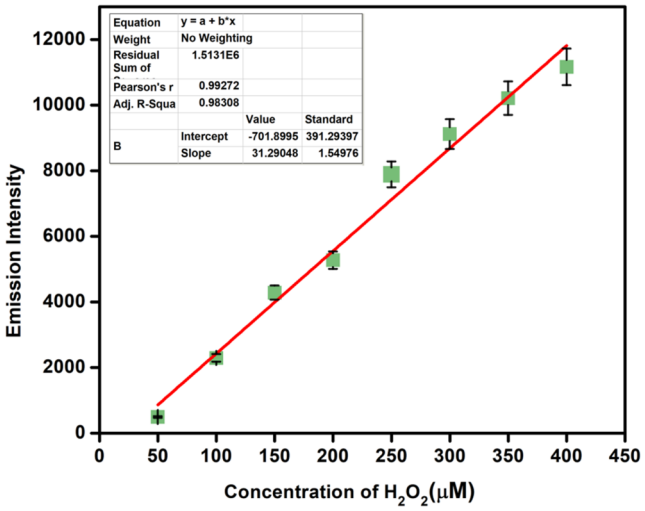

Figure 5. Plot for the calculation of LOD from the emission of **9** (10 μM, methanol/water: v/v = 70:30) with increasing concentrations of H_2O_2 (0−400 μM) (λ_{ex} = 485 nm and λ_{em} = 525 nm).

To assess the redox capacity of Se in probe **9**, the probe was initially oxidized with H_2O_2 and subsequently treated with biothiol glutathione. A significant decrease in the fluorescence emission intensity was observed, affirming the reversibility of probe **9**. The reduced probe was then further oxidized with H_2O_2 and a significant increase in fluorescent intensity was observed (Figure 6, cycle first). This process was analyzed for four cycles (cycles 1st−4th) for the alternate addition of H_2O_2 and glutathione.

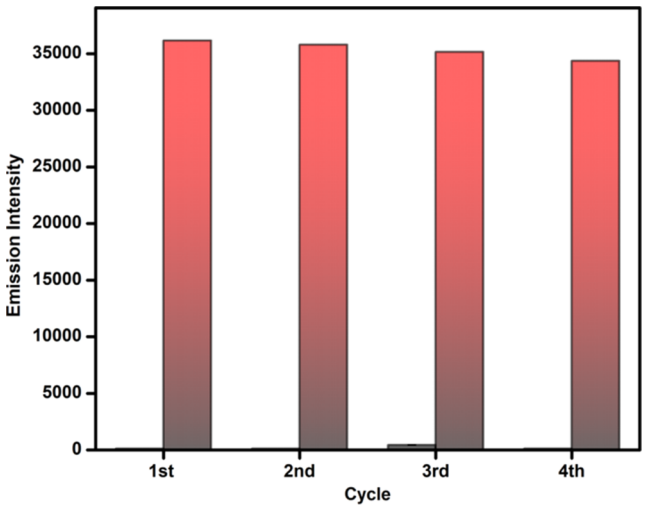

Figure 6. Fluorescence response before and after the addition of glutathione to the solution of probe **9** (10 μM, methanol/water: v/v = 70:30) and H_2O_2 (λ_{ex} = 485 nm and λ_{em} = 525 nm).

A pH-dependent experiment was performed with probe **9** to determine the optimal range for H_2O_2 sensing. The emission intensities of probe **9** are significantly low within the pH range of 2−12 (Figure 7). Upon the addition of H_2O_2, a notable

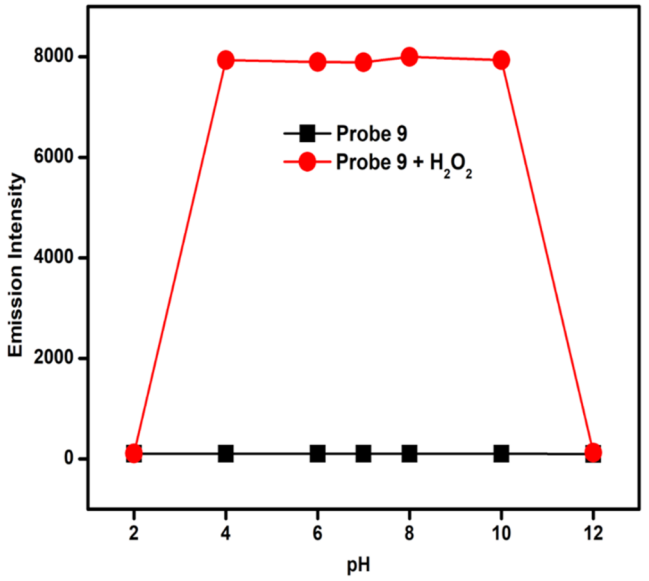

Figure 7. Fluorescence intensity measurements on probe **9** (10 μM) and the probe in the presence of 300 μM H_2O_2 under different pH ranges, λ_{ex} = 485 nm and λ_{em} = 525 nm.

increase in emission intensity at 525 nm was observed within a pH range of 4−10, which means that the probe could be used to detect H_2O_2 at the pH range of 4−10. At pH 12, the probe in the presence of H_2O_2 remains nonfluorescent.

An interference study was conducted for probe **9** in the presence of H_2O_2 and various other ROSs (*t*-BuOK, NO_3^-, ^-OCl, and KO_2) in Figure 8. The interferents such as *t*-BuOK, NO_3^-, OCl^-, and KO_2 have been included based on their potential to interact with the target probe **9**, potentially affecting the accuracy and reliability of the results. No significant change in the fluorescence intensity of the probe with H_2O_2 was observed in the presence of other ROSs. These

https://doi.org/10.1021/acsomega.4c05366
ACS Omega 2025, 10, 6396−6405

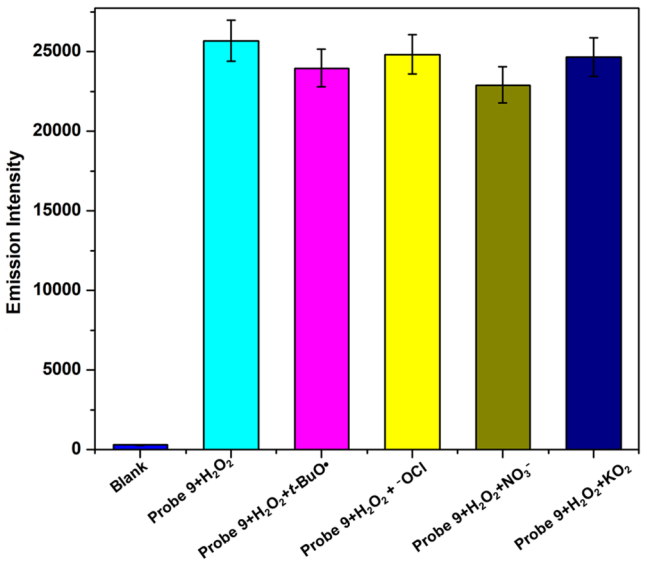

Figure 8. Fluorescence spectra of probe **9** (10 μM, methanol/water 70:30) and H_2O_2 with other ROS (*t*-BuOK, NO_3^-, ^-OCl, KO_2) (λ_{ex} = 485 nm and λ_{em} = 525 nm).

results indicate that other ROSs do not interfere with the detection of H_2O_2 by probe **9**.

Density functional theory (DFT) calculations were carried out to provide theoretical support for the experimentally observed "turn-on" fluorescence response during the detection of H_2O_2 and *t*-BuOOH. The geometry of probe **9** was fully optimized at the B3LYP/6-311+G(d,p) level of theory in the gas phase as shown in Figure 9 (see Table S8).

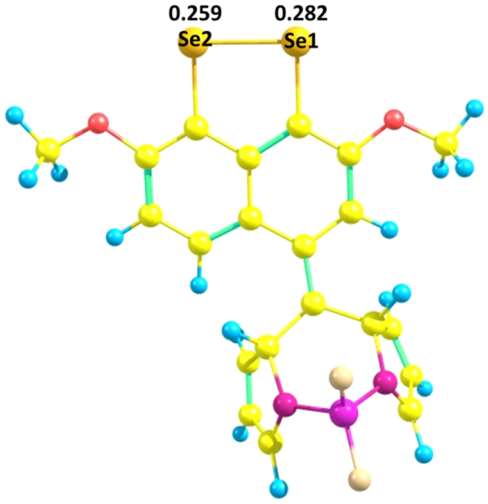

Figure 9. Optimized geometry of probe **9**.

Natural bond orbital (NBO) analysis at the B3LYP/6-311++G(d,p) level was used to investigate the charge density on the Se atoms, employing the B3LYP/6-311+G(d,p) level-optimized geometry. The analysis indicated that Se1 and Se2 exhibited positive charge densities of 0.282 and 0.259, respectively (Figure S23). Additionally, in the $^{77}Se\{^1H\}$ NMR spectrum of probe **9**, two signals at 426 and 418 ppm were observed, corresponding to Se1 and Se2, respectively. The analysis indicated that Se1 was more electron deficient than Se2. Based on the observed higher positive charge density on Se1, it was predicted that nucleophilic attack by H_2O_2/*t*-BuOOH would occur preferentially at this site.

A plausible mechanism for a "turn-on" event for probe **9** has been proposed as shown in Scheme 2.

In the proposed mechanism, electron transfer from the Se center to the BODIPY moiety resulted in PET quenching. As suggested from NBO analysis, the nucleophile H_2O_2/*t*-BuOOH attacked on the electron-deficient Se1 center. Further, intramolecular proton transfer would take place within intermediate **I** to produce intermediate **II**. Intermediate **II** rearranged to generate selenoxide **III** along with the elimination of the water/butyl alcohol molecule. The formation of selenoxide intermediate **III** was confirmed by the mass spectrum analysis of a mixture of probe **9** with H_2O_2. The isotopic pattern of Se with monooxidation was observed (see Figure S24). It was concluded that Se1(II) would oxidize to Se1(IV) and there was no electron density for transfer from the Se center to the BODIPY moiety. Thus, the PET mechanism was blocked and significant enhancement in fluorescence intensity was observed. The PET mechanism is well documented in previous research studies.[33,42]

To provide further evidence for the occurrence of PET quenching, the frontier molecular orbitals (FMOs) of probe **9** and its oxidized form, selenoxide **III**, were investigated and are depicted in Figure 10 (see also Figures S25 and S26). The geometry of selenoxide **III** was fully optimized at the B3LYP/6-311+G(d,p) level of theory (see Table S8).

Analysis of the frontier molecular orbitals revealed that the highest occupied molecular orbital (HOMO) of probe 9 was primarily localized on the naphthalene core, whereas the lowest unoccupied molecular orbital (LUMO) was predominantly localized on the BODIPY core (Figure 10A). Electron transfer from HOMO to LUMO of probe **9** corresponded to its quenched state.[32] However, in selenoxide **III**, sustained electron density was observed within both HOMO and LUMO of the BODIPY core (Figure 10B). Consequently, this alteration led to a significant enhancement in the fluorescence intensity exhibited by probe **9**.

CONCLUSIONS

In summary, probe **9** was developed for the selective and sensitive detection of H_2O_2 and *t*-BuOOH, $^{\bullet}OH$, and $ONOO^-$. H_2O_2, *t*-BuOOH, $^{\bullet}OH$, and $ONOO^-$ were the species that showed a significant increase in fluorescence intensity in the absorption spectra. The probe's oxidized form was reversibly generated with glutathione. The "turn-on" mechanism was proposed and supported with the DFT calculations. This study aims to investigate the potential application of a small organoselenium molecular probe for the detection of H_2O_2, *t*-BuOOH, $^{\bullet}OH$, and $ONOO^-$ in living organisms.

EXPERIMENTAL SECTION

All reactions were monitored by TLC using a UV lamp (λ = 254 nm). ^1H and $^{13}C\{^1H\}$ NMR spectra for all synthesized products were recorded on 400 MHz (^1H: 400 MHz, $^{13}C\{^1H\}$: 100 MHz) and 500 MHz (^1H: 500 MHz, $^{13}C\{^1H\}$: 125 MHz) spectrometer. Solvent residual peaks were used as an indirect reference to tetramethylsilane (TMS) (δ = 0 ppm), i.e., $CDCl_3$ (^1H: δ = 7.26; ^{13}C: δ = 77.2 ppm) and DMSO-d_6 (^1H: δ = 2.50; ^{13}C: δ = 39.5 ppm). The $^{77}Se\{^1H\}$ NMR spectra were obtained on a 500 MHz ($^{77}Se\{^1H\}$: 100 MHz) spectrometer,

https://doi.org/10.1021/acsomega.4c05366
ACS Omega 2025, 10, 6396−6405

Scheme 2. Proposed Mechanism for the "Turn-on" Response of Probe 9 with H_2O_2 and *t*-BuOOH

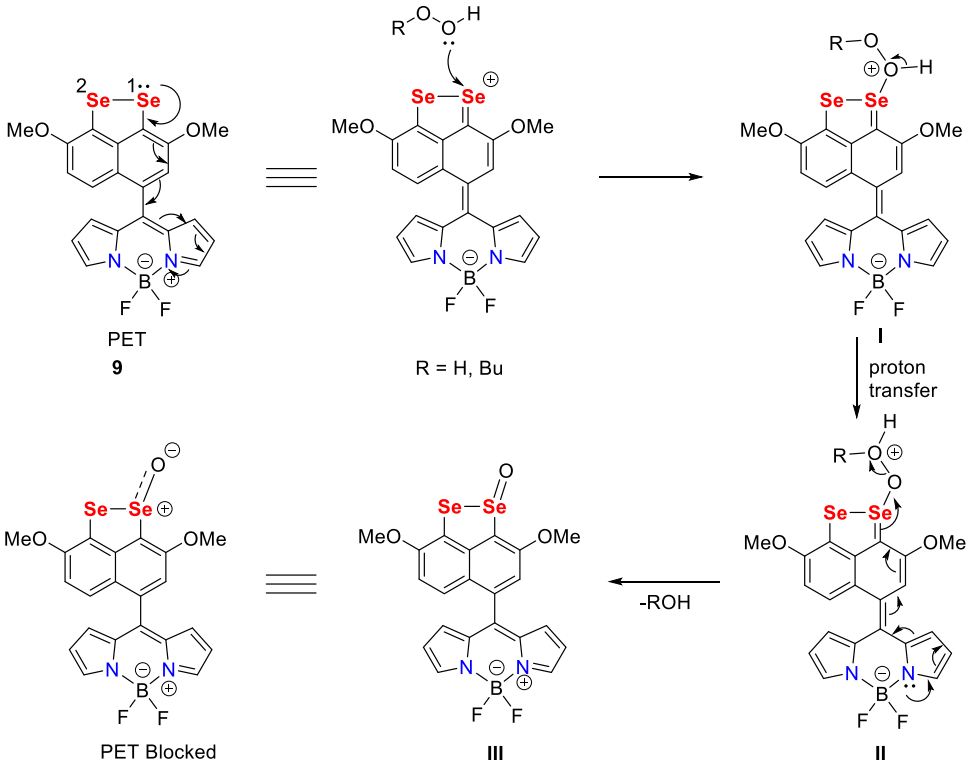

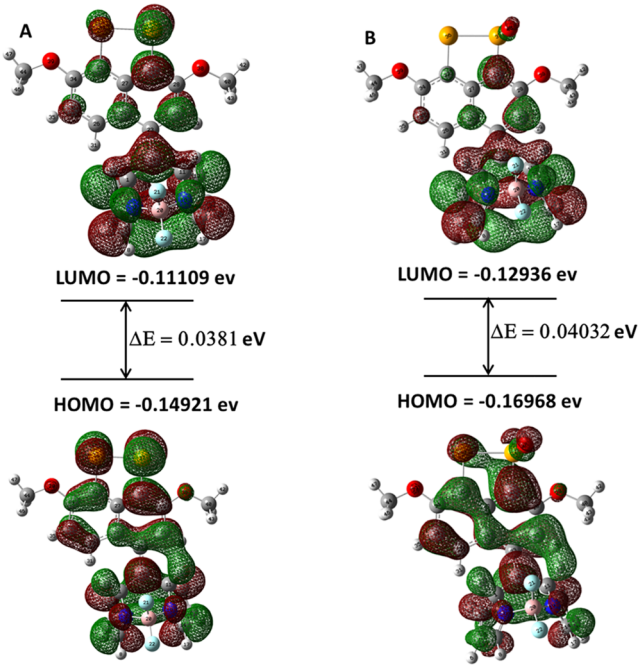

Figure 10. HOMO and LUMO of (A) probe **9**; (B) selenoxide **III** in gas phase calculations (B3LYP/6-311G+(d,p)).

using Ph_2Se_2 (δ = 463 ppm) as an indirect reference to Me_2Se (δ = 0 ppm). For purification, silica gel (60−120 mesh) size was utilized in flash column chromatography. The melting points for all compounds were determined without corrections using a digital melting point apparatus. HRMS spectra were acquired on a time-of-flight (TOF) mass spectrometer with electrospray ionization (ESI) in positive ion mode. A Cary 5000 UV−vis−NIR spectrophotometer was employed for absorption measurements, and fluorescence spectra were recorded on a PerkinElmer FL6500 spectrophotometer.

Synthesis of 2,7-Dimethoxynaphtho[1,8-cd]-1,2-diselenole (6).[39] *n*-Butyllithium (4 mL, 2.0 M, 8 mmol) was added to a solution of 1,8-dibromo-2,7-dimethoxynaphthalene (1.0 g, 2.88 mmol) in dry THF at −78 °C under an inert atmosphere (N_2). After 1.5 h of the reaction, elemental Se was introduced at 0 °C and the reaction mixture was further allowed to stir overnight at room temperature. The solution was quenched with ammonium chloride and stirred for 0.5 h in open air. The organic layer was extracted with dichloromethane (DCM, 3 × 20 mL) and washed with brine. The combined organic layers were dried over anhydrous sodium sulfate (Na_2SO_4) and concentrated under reduced pressure. Purification was performed using column chromatography and ethyl acetate/*n*-hexane (4%) as an eluent, affording diselenide **6**. Yield: 0.45 g (55%), mp 150−151 °C (mp 155−156 °C, literature); purple solid. ^{1}H NMR (400 MHz, $CDCl_3$) δ 7.60 (s, 1H), 6.98 (d, J = 8.72 Hz, 1H), 4.49 (d, J = 18.8 Hz, 3H) 1.64 (s, 3H).

Synthesis of *p*-Formylnaphthyl Diselenide 7. Diselenide **6** (0.3 g, 0.87 mmol) was dissolved in dry DCM and $POCl_3$ (0.23 g, 0.14 mL, 1.5 mmol) was added dropwise at 0 °C. The reaction mixture was then heated at 50 °C for overnight. After the completion of the reaction, it was quenched with water and extracted with ethyl acetate (3 × 20 mL), washed with brine solution, dried over anhydrous Na_2SO_4, and concentrated under reduced pressure, resulting in a red-colored residue. Purification was performed using column chromatography and ethyl acetate/*n*-hexane (4%) as an eluent. Orange-colored compound **7** was obtained as a product. Yield: 0.28 g (87%), m.p.: 214−216 °C. ^{1}H NMR (500 MHz, $CDCl_3$) δ 10.25 (s, 1H), 8.97 (d, J = 10.0 Hz, 1H), 7.41 (s, 1H), 7.17 (d, J = 10.0 Hz, 1H), 4.06 (s, 3H), 4.03 (s,

https://doi.org/10.1021/acsomega.4c05366
ACS Omega 2025, 10, 6396−6405

3H). $^{13}C\{^1H\}$ NMR (125 MHz, $CDCl_3$) δ 191.0, 153.7, 152.2, 140.9, 136.3, 129.9, 125.4, 124.2, 123.2, 119.9, 113.5, 56.6, 56.5. $^{77}Se\{^1H\}$ NMR (100 MHz, $CDCl_3$) δ 448, 429. HRMS (ESI/TOF) m/z $[M]^+$ calcd. for $C_{13}H_{10}O_3Se_2$, 373.8960, found 373.8943.

Synthesis of Dipyrrolemethane Diselenide 8. To the solution of diselenide **7** (0.35 g, 0.94 mmol), pyrrole (3 mL) and a catalytic amount of TFA (0.05 mL) were added. The reaction mixture was allowed to stir for 6 h at room temperature. The progress of the reaction was monitored by TLC. After completion of the reaction, it was quenched with water and extracted with DCM (3 × 20 mL). The combined organic layers were dried over anhydrous Na_2SO_4 and evaporated to dryness under reduced pressure using a rotary evaporator. Purification was performed using column chromatography and ethyl acetate/*n*-hexane (10%) as an eluent, affording purple color compound **8** as a product. Yield: 0.34 g (76%), m.p.: >300 °C. ^1H NMR (500 MHz, DMSO-d_6) δ 7.83 (d, J = 5.0 Hz, 1H), 7.15 (d, J = 10.0 Hz, 1H), 6.74 (s, 1H), 6.62 (s, 2H), 5.96 (s, 1H), 5.90 (m, 2H), 5.67 (s, 2H), 3.93 (s, 3H), 3.74 (s, 3H). $^{13}C\{^1H\}$ NMR (125 MHz, DMSO-d_6) δ: 153.1, 152.6, 140.2, 139.6, 132.9, 126.1, 123.2, 122.5, 120.5, 117.4, 112.4, 112.3, 107.4, 107.0, 56.8, 56.5. $^{77}Se\{^1H\}$ NMR (100 MHz, DMSO-d_6) δ 407, 398. HRMS (ESI/TOF) m/z $[M]^+$ calcd. for $C_{21}H_{18}N_2O_2Se_2$, 489.9699, found 489.9690.

Synthesis of Cyclic Diselenide-BODIPY Probe 9. DDQ (0.33 g, 1.43 mmol) was added to the solution of dipyrrolemethane diselenide **8** (0.35 g, 0.72 mmol) in DCM (20 mL), and the mixture was stirred at RT for 45 min under nitrogen atmosphere. NEt_3 (2.06 mL, 14.75 mmol) was added to the mixture and the reaction mixture was allowed to stir for 10 min, followed by the addition of 14.75 mmol $BF_3{\cdot}Et_2O$ (1.82 mL) and the reaction was left to stir for 3 h at room temperature. The progress of the reaction was monitored by TLC. After completion of the reaction, the reaction was quenched with water and extracted with DCM (3 × 20 mL). The combined organic layers were dried over anhydrous Na_2SO_4 and evaporated to dryness under reduced pressure using a rotary evaporator. Purification was performed using column chromatography and ethyl acetate/*n*-hexane (6−10%) as an eluent, affording green-colored solid compound **8** as a product. Yield: 0.24 g (63%), m.p.: 234−236 °C; IR (KBr) 3142, 1545,1389, 1256, 782, 581 cm^{-1}. ^1H NMR (500 MHz, DMSO-d_6) δ 8.15 (s, 2H), 7.35 (d, J = 6.5 Hz, 2H), 7.09 (d, J = 9.5 Hz, 1H), 6.83 (d, J = 3.5 Hz, 2H), 6.57 (d, J = 2.5 Hz, 2H), 3.95 (s, 3H), 3.89 (s, 3H). $^{13}C\{^1H\}$ NMR (125 MHz, DMSO-d_6) δ: 152.8, 151.7, 145.0, 144.5, 139.5, 135.0, 131.1, 128.3, 126.3, 126.1, 123.5, 122.3, 119.2, 114.6, 112.6, 56.7, 56.3. $^{77}Se\{^1H\}$ NMR (100 MHz, DMSO-d_6) δ 426, 418. HRMS (ESI/TOF) m/z $[M]^+$ calcd. for $C_{21}H_{15}BF_2N_2O_2Se_2$, 535.9525, found 535.9513. FTIR (KBr) 3142, 1545, 1389, 1256, 1057, 782, 581 cm^{-1}.

X-ray Crystallographic Study. X-ray crystallographic study of compound **6** was performed using graphite-monochromatized Mo−Kα radiation (λ = 0.71073 Å). The single crystal of compound **6** was mounted on a SuperNova, Single source at offset/far, HyPix3000 diffractometer. Data collection was carried out at 293(2) K. The structure of the compound was solved using Olex2[43] and refined through a full-matrix least-squares procedure on F^2 for all reflections with SHELXL-2016 software.[44] Hydrogen atoms were positioned by geometrical means and refined using a riding model. Their isotropic thermal parameters were set at 1.5 times U(eq) of the corresponding carbon atoms for sp^3 C−H bonds and 1.2 times U(eq) of the corresponding carbon atoms for sp^2 C−H bonds. The crystallographic data associated with the structure presented in this study have been archived with the Cambridge Crystallographic Data Centre (CCDC) under accession number CCDC 2322340 (compound **6**). These data can be obtained free of charge from CCDC. Data for compound **6**: $C_{24}H_{20}O_4Se_4$, M_r = 688.24, monoclinic, space group $P2_1/n$, a = 11.9484(3) Å, b = 12.3700(4) Å, c = 16.1224(4) Å, α = 90°, β = 102.636(3)°, γ = 90°, V = 2325.20(11) $Å^3$, Z = 4, T = 293(2) K, $\rho_{(calcd)}$ = 1.966 g/cm^3, GOF = 1.067, R_1 = 0.0742, wR_2 = 0.1196 ($I > 2\sigma(I)$); R_1 = 0.1403, wR_2 = 0.1367 (all data). Of the 30,471 reflections that were measured, 5009 were unique (R_{int} = 0.0909).

Photophysical Study. *Details of UV−Vis and Fluorescence Measurements.* The emission of probe **9** was measured using spectrophotometric titration in a mixture of methanol and water. The stock solution of probe **9** (10 μM) was prepared in methanol/water (v/v = 70:30; 10 μM). ROSs/RNSs ($^-$OCl, $O_2^{\bullet-}$, H_2O_2, *t*-BuOOH, *t*-BuO$^\bullet$, $^\bullet$OH, $ONOO^-$) were prepared at a concentration of 10 mM in distilled water. A 5 mL sample of probe **9** (10 μM) was mixed with these ROSs, and the probe's emission was subsequently measured. The λ_{max} absorption for probe **9** was 500 nm and probe **9** was excited at λ_{max} emission of 525 nm. The graphs were plotted using Origin 2019b.

*Evaluation of Probe **9** for ROSs: Screening and Sensitivity Studies.* Probe **9** was subjected to the screen with different ROSs/RNSs, including $^-$OCl, $O_2^{\bullet-}$, H_2O_2, *t*-BuOOH, *t*-BuO$^\bullet$, $^\bullet$OH, $ONOO^-$, glutathione, and ascorbic acid. For this experimental procedure, 5 mL of probe **9** at a concentration of 10 μM was combined with ROSs in water. The photometric titration experiment involved gradually increasing the concentration of H_2O_2, *t*-BuOOH, $^\bullet$OH, and $ONOO^-$ (ranging from 0 to 400 μM). UV−vis and fluorescence measurements were subsequently performed after mixing.

Determination of the Detection Limit. The determination of the LOD values was carried out by analyzing the fluorescence concentration curve. The fluorescence emission spectrum of probe **9** was measured three times, and the standard deviation of the seven blank measurements was calculated. To determine the slope, the fluorescence intensity at a specific wavelength of 525 nm was plotted against the concentrations of H_2O_2, *t*-BuOOH, $^\bullet$OH, and $ONOO^-$. The limit of detection was determined using the following equation:

$$\text{limit of detection} = 3\sigma/k$$

where σ represents the standard deviation of seven blank measurements and k is the slope relating fluorescence intensity to the concentrations of H_2O_2, *t*-BuOOH, $^\bullet$OH, and $ONOO^-$.

Computational Details. All geometrical calculations were performed using the Gaussian 09 suite of quantum chemistry software.[45] Density functional theory (DFT) calculations were conducted using the hybrid Becke 3 Lee−Yang−Parr (B3LYP) exchange-correlation functional.[46] The geometry optimization was carried out with the B3LYP/6-311+G(d,p) basis sets. The charge on the Se atoms was evaluated by natural bond orbital (NBO) analysis at the B3LYP/6-311++G(d,p) level.[47]

https://doi.org/10.1021/acsomega.4c05366
ACS Omega 2025, 10, 6396−6405

■ ASSOCIATED CONTENT

Data Availability Statement

The data that support the findings of this study are available in the Supporting Information.

Supporting Information

The Supporting Information is available free of charge at https://pubs.acs.org/doi/10.1021/acsomega.4c05366.

^{1}H, ^{13}C{^{1}H}, ^{77}Se{^{1}H} NMR, and HRMS spectra for all new compounds; UV−vis and fluorescence spectra (PDF)

■ AUTHOR INFORMATION

Corresponding Authors

Jamal Rafique − *LabSO, Instituto de Química − IQ, Universidade Federal de Goiás − UFG, Goiânia 74690-900 GO, Brazil; Instituto de Química − INQUI, Universidade Federal do Mato Grosso do Sul − UFMS, Campo Grande 79074-460 MS, Brazil;* orcid.org/0000-0002-2336-040X; Email: jamal.rafique@ufms.br

Sumbal Saba − *LabSO, Instituto de Química − IQ, Universidade Federal de Goiás − UFG, Goiânia 74690-900 GO, Brazil;* orcid.org/0000-0002-6134-7249; Email: sumbalsaba@ufg.br

Vijay P. Singh − *Department of Chemistry & Centre of Advanced Studies in Chemistry, Panjab University, Chandigarh 160014, India; Instituto de Química − INQUI, Universidade Federal do Mato Grosso do Sul − UFMS, Campo Grande 79074-460 MS, Brazil;* orcid.org/0000-0002-5584-2067; Email: vijay@pu.ac.in

Authors

Babli Chhillar − *Department of Chemistry & Centre of Advanced Studies in Chemistry, Panjab University, Chandigarh 160014, India*

Nikhil Sodhi − *Department of Chemistry & Centre of Advanced Studies in Chemistry, Panjab University, Chandigarh 160014, India*

Rajni Kadian − *Department of Chemistry & Centre of Advanced Studies in Chemistry, Panjab University, Chandigarh 160014, India*

Eliane Ribeiro Neres − *LabSO, Instituto de Química − IQ, Universidade Federal de Goiás − UFG, Goiânia 74690-900 GO, Brazil*

Manisha Yadav − *Department of Chemistry & Centre of Advanced Studies in Chemistry, Panjab University, Chandigarh 160014, India*

Manisha Kundu − *Department of Chemistry & Centre of Advanced Studies in Chemistry, Panjab University, Chandigarh 160014, India*

Vinutha K. Venkatareddy − *Department of Chemistry, Indian Institute of Technology Dharwad, Dharwad 580011 Karnataka, India*

Rajeswara Rao Malakalapalli − *Department of Chemistry, Indian Institute of Technology Dharwad, Dharwad 580011 Karnataka, India;* orcid.org/0000-0003-2730-7275

Complete contact information is available at: https://pubs.acs.org/10.1021/acsomega.4c05366

Author Contributions

Conceptualization: S.S. and V.P.S.; Methodology: B.C., N.S., R.K., E.R.N., M.Y., and M.K.; Validation: B.C., N.S., R.K., E.R.N., M.Y., and M.K.; Formal analysis: B.C., N.S., R.K., E.R.N., M.Y., and M.K.; Investigation: B.C., N.S., R.K., E.R.N., M.Y., and M.K.; Resources: J.R., S.S., and V.P.S.; Data curation: B.C., N.S., V.K.V., and R.R.M.; Writing - Original draft: B.C. and V.P.S.; Writing - Review and Editing: J.R., S.S., and V.P.S.; Visualization: J.R., S.S., and V.P.S.; Supervision: S.S. and V.P.S.; Project administration: J.R., S.S., and V.P.S.; Funding acquisition: J.R., S.S., and V.P.S. All authors read and approved the final draft of the manuscript.

Funding

The Article Processing Charge for the publication of this research was funded by the Coordination for the Improvement of Higher Education Personnel - CAPES (ROR identifier: 00x0ma614).

Notes

The authors declare no competing financial interest.

■ ACKNOWLEDGMENTS

The Council of Scientific and Industrial Research (CSIR), New Delhi, is acknowledged for the financial support with Grant No. 01(3074)/21/EMR-II and the Science of Engineering and Research Board (SUR/2022/002214). B.C. is thankful to CSIR, New Delhi, for the fellowship. We gratefully acknowledge the Department of Chemistry & Centre of Advanced Studies in Chemistry, Panjab University, Chandigarh, CNPq Brazil, CAPES (Finance Code 001) Brazil. J.R. and S.S. would like to acknowledge CNPq (316687/2023-5, 309975/2022-0, 404172/2023-7, and 405655/2023-1). S.S. would also like to acknowledge FAPEG (04/2023; EQU2023101000020).

■ REFERENCES

(1) Mugesh, G.; du Mont, W. W.; Sies, H. Chemistry of biologically important synthetic organoselenium compounds. *Chem. Rev.* **2001**, *101*, 2125−2180.

(2) (a) Arsenyan, P.; Rubina, K.; Shestakova, I.; Domracheva, I. 4-Methyl-1,2,3-selenadiazole-5-carboxylic acid amides: Antitumor action and cytotoxic effect correlation. *Eur. J. Med. Chem.* **2007**, *42*, 635−640. (b) Veloso, I. C.; Delanogarie, E.; Machado, A. E.; Braga, S. P.; Rosa, G. K.; de Bem, A. F.; Rafique, J.; Saba, S.; da Trindade, R. N.; Galetto, F. Z.; Moreria, E. L. G. A selanylimidazopyridine (3-SePh-IP) reverses the prodepressant-and anxiogenic-like effects of a high-fat/high-fructose diet in mice. *J. Pharm. Pharmacol.* **2021**, *73*, 673−681. (c) Rafique, J.; Farias, G.; Saba, S.; Zapp, E.; Bellettini, I. C.; Salla, C. A. M.; Bechtold, I. H.; Scheide, M. R.; Neto, J. S. S.; Souza, D. M., Jr.; Braga, H. C.; Ribeiro, L. F. B.; Gastaldon, F.; Pich, C. T.; Frizon, T. E. A. Selenylated-oxadiazoles as promising DNA intercalators: Synthesis, electronic structure, DNA interaction and cleavage. *Dyes Pigm.* **2020**, *180*, 108519−108529.

(3) (a) Gomes, G. B.; Zubieta, C. S.; Guilhermi, J. S.; Toffoli-Kadri, M. C.; Beatriz, A.; Rafique, J.; Parisotto, E. B.; Saba, S.; Perdomo, R. T. Selenylated imidazo [1,2-a]pyridine induces apoptosis and oxidative stress in 2D and 3D models of colon cancer cells. *Pharmaceuticals* **2023**, *16*, 814−829. (b) dos Santos, D. C.; Rafique, J.; Saba, S.; Almeida, G. M.; Siminski, T.; Padua, C.; Filho, D. W.; Zamoner, A.; Braga, A. L.; Pedrosoa, R. C.; Ourique, F. Apoptosis oxidative damage-mediated and antiproliferative effect of selenylated imidazo[1,2-a]pyridines on hepatocellular carcinoma HepG2 cells and in vivo. *J. Biochem. Mol. Toxicol.* **2021**, *35*, e22663. (c) dos Santos, D. C.; Rafique, J.; Saba, S.; Grinevicius, V. M. A. S.; Filho, D. W.; Zamoner, A.; Braga, A. L.; Pedrosa, R. C.; Ourique, F. IP-Se-06, a selenylated imidazo[1,2-a]pyridine, modulates intracellular redox state and causes Akt/mTOR/HIF-1α and MAPK signaling inhibition, promoting antiproliferative effect and apoptosis in glioblastoma cells. *Oxid. Med. Cell. Longevity* **2022**, *2022*, No. 3710449.

(4) Mukherjee, A. J.; Zade, S. S.; Singh, H. B.; Sunoj, R. B. Organoselenium chemistry: role of intramolecular interactions. *Chem. Rev.* **2010**, *110*, 4357−4416.
(5) *Selenium: Its Molecular Biology and Role in Human Health*, 3rd ed.; Hatfield, D. L.; Berry, M. J.; Gladyshev, V. N.; Eds, D. L.; Hatfield, M. J.; Berry, V. N.; Gladyshev, V. N., Eds.; Springer-Verlag: New York, 2012.
(6) Mugesh, G.; Panda, A.; Singh, H. B.; Punekar, N. S.; Butcher, R. J. Glutathione peroxidase-like antioxidant activity of diaryl diselenides: a mechanistic study. *J. Am. Chem. Soc.* **2001**, *123*, 839−850.
(7) (a) Botteselle, G. V.; Elias, W. C.; Bettanin, L.; Canto, R. F. S.; Domingos, D. N. O.; Rafique, J.; Braga, A. L.; et al. Catalytic antioxidant activity of bis-aniline-derived diselenides as GPx mimics. *Molecules* **2021**, *26*, 4446. (b) Scheide, M. R.; Peterle, M. M.; Saba, S.; Neto, J. S. S.; Lenz, G. F.; Cezar, R. D.; Felix, J. F.; Botteselle, G. V.; Schneider, R.; Rafique, J.; Braga, A. L. Catalyst- and metal-free C(sp2)−H bond selenylation of (N-hetero)-arenes using diselenides and trichloroisocyanuric acid at room temperature. *Sci. Rep.* **2020**, *10*, No. 15233.
(8) Yadav, M.; Kumar, M.; Chahal, A.; Sodhi, N.; Chhillar, B.; Alajangi, H. K.; Barnwal, R. P.; Singh, V. P. Synthesis, reactions, and antioxidant properties of bis (3-amino-1-hydroxybenzyl) diselenide. *J. Org. Chem.* **2023**, *88*, 3509−3522.
(9) Yadav, M.; Singh, V. P. Glutathione peroxidase-like antioxidant activity of 1,3-benzoselenazoles: Synthesis and in silico molecular docking studies as pancreatic lipase inhibitors. *J. Org. Chem.* **2023**, *88*, 16934−16948.
(10) Kumar, M.; Chhillar, B.; Verma, D.; Nain, S.; Singh, V. P. Introduction of methyl group in substituted isoselenazolones: catalytic and mechanistic study. *J. Org. Chem.* **2023**, *88*, 4273−4285.
(11) Chhillar, B.; Kadian, R.; Kumar, M.; Yadav, M.; Sodhi, N.; da Silva, T. N. X.; Angeli, J. P. F.; Singh, V. P. Aminic organoselenium compounds as glutathione peroxidase mimics and inhibitors of ferroptosis. *ChemBioChem* **2024**, *25*, No. e202400074.
(12) Chhillar, B.; Sharma, A.; Rani, S.; Singh, G.; Barnwal, R. P.; Singh, V. P. Synthesis of *bis*-naphthol based organoselenium antioxidants as efficient inhibitors against biofilms. *ChemistrySelect* **2024**, *9*, No. e202305025.
(13) (a) Malankar, G. S.; Shelar, D. S.; Manikandan, M.; Patra, M.; Manjare, S. T. Synthesis of selenium-based BOPHY sensor for imaging of Cu(II) in living HeLa cells. *J. Mol. Struct.* **2023**, *1281*, No. 135118. (b) Salunke, S. T.; Shelar, D. S.; Salunkhe, S. S.; et al. Organoselenium-based quinoline sensor for superoxide detection and its antitumor activities. *J. Chem. Sci.* **2024**, *136*, 51. (c) Shelar, D. S.; Malankar, G. S.; Salunke, S. S.; Manikandan, M.; Chavan, A. D.; Pinjari, R. V.; Patra, M.; Butcher, R. J.; Manjare, S. T. Synthesis and characterization of organoselenium based BODIPY and its application in living cells. *Bioorg. Chem.* **2024**, *150*, 107568.
(14) Mamgain, R.; Singh, F. V. Selenium-based fluorescence probes for the detection of bioactive molecules. *ACS Org. Inorg. Au* **2022**, *2*, 262−288.
(15) (a) Singh, A. P.; Lee, K. M.; Murale, D. P.; Jun, T.; Liew, H.; Suh, Y.- H.; Churchill, D. G. Novel sulphur-rich BODIPY systems that enable stepwise fluorescent O-atom turn-on and H_2O_2 neuronal system probing. *Chem. Commun.* **2012**, *48*, 7298−7300. (b) Ahrens, J.; Boker, B.; Brandhorst, K.; Funk, M.; Broring, M. Sulfur-Bridged BODIPY DYEmers. *Chem. − Eur. J.* **2013**, *19*, 11382−11395.
(16) (a) Koide, Y.; Kawaguchi, M.; Urano, Y.; Hanaoka, K.; Komatsu, T.; Abo, M.; Terai, T.; Nagano, T. A reversible near-infrared fluorescence probe for reactive oxygen species based on Te−rhodamine. *Chem. Commun.* **2012**, *48*, 3091−3093. (b) Singh, A.; Dhau, J.; Kumar, R.; Badru, R.; Kaushik, A. Exploring the fluorescence properties of tellurium-containing molecules and their advanced applications. *Phys. Chem. Chem. Phys.* **2024**, *26*, 9816−9847.
(17) Malankar, G. S.; Cugnasca, B. S.; Wodtke, F.; de Albuquerque, J. L. P.; Deshmukh, P. P.; Shelar, D. S.; Santos, A. A. D.; Manjare, S. T. *Chalcogen Chemistry: Fundamentals and Applications*; Lippolis, V.; Santi, C.; Lenardão, E. J.; Braga, A. L., Eds.; The Royal Society of Chemistry, 2023; Vol. *14*, pp 384−418.
(18) Valko, M.; Rhodes, C. J. B.; Moncol, J.; Izakovic, M. M.; Mazur, M. Free radicals, metals and antioxidants in oxidative stress-induced cancer. *Chem.−Biol. Interact.* **2006**, *160*, 1−40.
(19) Anik, M. I.; Mahumad, N.; Masud, A. A.; Khan, I. M.; Islam, N. M.; Uddin, S.; Hossain, K. M. Role of reactive oxygen species in aging and age-related diseases: a review. *ACS Appl. Bio Mater.* **2022**, *5*, 4028−4054.
(20) Valko, M.; Leibfritz, D.; Moncol, J.; Cronin, M. T. D.; Mazur, M.; Telser, J. Free radicals and antioxidants in normal physiological functions and human disease. *Int. J. Biochem. Cell Biol.* **2007**, *39*, 44−84.
(21) Kepp, K. P. Bioinorganic chemistry of Alzheimer's disease. *Chem. Rev.* **2012**, *112*, 5193−5239.
(22) Yap, Y. W.; Whiteman, M.; Cheung, N. S. Chlorinative stress: an underappreciated mediator of neurodegeneration? *Cell. Signal.* **2007**, *19*, 219−228.
(23) Lou, Z.; Li, P.; Han, K. Redox-responsive fluorescent probes with different design strategies. *Acc. Chem. Res.* **2015**, *48*, 1358−1368.
(24) Rabut, G.; Ellenberg, J. Automatic real-time three-dimensional cell tracking by fluorescence microscopy. *J. Microsc.* **2004**, *216*, 131−137.
(25) Du, J.; Hu, M.; Fan, J.; Peng, X. Fluorescent chemodosimeters using "mild" chemical events for the detection of small anions and cations in biological and environmental media. *Chem. Soc. Rev.* **2012**, *41*, 4511−4535.
(26) (a) Manjare, S. T.; Kim, Y.; Churchill, D. G. Selenium-and tellurium-containing fluorescent molecular probes for the detection of biologically important analytes. *Acc. Chem. Res.* **2014**, *47*, 2985−2998. (b) Salunke, S. T.; Shelar, D. S.; Manjare, S. T. Synthesis and photophysical study of tetraphenyl substituted BODIPY based phenyl-monoselenide probe for selective detection of superoxide. *J. Fluoresc.* **2023**, *33*, 437−444. (c) Bozzi, I. A. O.; Machado, L. A.; Diogo, E. B. T.; Delolo, F. G.; Barros, L. O. F.; Graca, G. A. P.; Araujo, M. H.; Martins, F. T.; Pedrosa, L. F.; da Luz, L. C.; Moraes, E. S.; Rodembusch, F. S.; Guimaraes, J. S. F.; Oliveira, A. G.; Rotteger, S. H.; Werz, D. B.; Souza, C. P.; Fantuzzi, F.; Han, J.; Marder, T. B.; Braunschweig, H.; da Silva Junior, E. N. Electrochemical Diselenation of BODIPY Fluorophores for Bioimaging Applications and Sensitization of $^1O_2$. *Chem. − Eur. J.* **2024**, *30*, e202303883.
(27) (a) Wang, B.; Yu, F.; Li, P.; Sun, X.; Han, K. A BODIPY fluorescence probe modulated by selenoxide spirocyclization reaction for peroxynitrite detection and imaging in living cells. *Dyes Pigm.* **2013**, *96*, 383−390. (b) Yu, F.; Li, P.; Wang, B.; Han, K. Reversible near-infrared fluorescent probe introducing tellurium to mimetic glutathione peroxidase for monitoring the redox cycles between peroxynitrite and glutathione in vivo. *J. Am. Chem. Soc.* **2013**, *135*, 7674−7680.
(28) (a) Zeng, X.; Zhang, X.; Zhu, B.; Jia, H.; Yang, W.; Li, Y.; Xue, J. A colorimetric and ratiometric fluorescent probe for quantitative detection of GSH at physiologically relevant levels. *Sens. Actuators, B* **2011**, *159*, 142−147. (b) Balkrishna, S. J.; Hodge, A. S.; Kumar, S.; Pani, I. P.; Kumar, S. Sensitive and regenerable organochalcogen probes for the colorimetric detection of thiols. *RSC Adv.* **2014**, *4*, 11535−11538.
(29) Loudet, A.; Burgess, K. BODIPY dyes and their derivatives: syntheses and spectroscopic properties. *Chem. Rev.* **2007**, *107*, 4891−4932.
(30) Ulrich, G.; Ziessel, R.; Harriman, A. The chemistry of fluorescent BODIPY dyes: versatility unsurpassed. *Angew. Chem., Int. Ed.* **2008**, *47*, 1184−1201.
(31) Bessette, A.; Hanan, G. S. Design, synthesis and photophysical studies of dipyrromethene-based materials: insights into their applications in organic photovoltaic devices. *Chem. Soc. Rev.* **2014**, *43*, 3342−3405.
(32) Chou, C. Y.; Liu, S. R.; Wu, S. P. A highly selective turn-on fluorescent sensor for Cu (II) based on an NSe_2 chelating moiety and its application in living cell imaging. *Analyst* **2013**, *138*, 3264−3270.

https://doi.org/10.1021/acsomega.4c05366
ACS Omega 2025, 10, 6396−6405

(33) Liu, S. R.; Wu, S. P. Hypochlorous acid turn-on fluorescent probe based on oxidation of diphenyl selenide. *Org. Lett.* **2013**, *15*, 878−881.
(34) Manjare, S. T.; Kim, J.; Lee, Y.; Churchill, D. G. Facile meso-BODIPY annulation and selective sensing of hypochlorite in water. *Org. Lett.* **2014**, *16*, 520−523.
(35) Mulay, S. V.; Choi, M.; Jang, Y. J.; Kim, Y.; Jon, S.; Churchill, D. G. Enhanced fluorescence turn-on imaging of hypochlorous acid in living immune and cancer cells. *Chem. − Eur. J.* **2016**, *22*, 9642−9648.
(36) Deshmukh, P. P.; Navalkar, A.; Maji, S. K.; Manjare, S. T. Phenylselenyl containing turn-on dibodipy probe for selective detection of superoxide in mammalian breast cancer cell line. *Sens. Actuators, B* **2019**, *281*, 8−13.
(37) Madibone, K. S.; Deshmukh, P. P.; Navalkar, A.; Maji, S. K.; Badani, P. M.; Manjare, S. T. Cyclic organoselenide BODIPY-based probe: targeting superoxide in MCF-7 cancer cells. *ACS Omega* **2020**, *5*, 14186−14193.
(38) (a) Lou, Z.; Li, P.; Sun, X.; Yang, S.; Wang, B.; Han, K. A fluorescent probe for rapid detection of thiols and imaging of thiols reducing repair and H_2O_2 oxidative stress cycles in living cells. *Chem. Commun.* **2013**, *49*, 391−393. (b) Xu, K.; Qiang, M.; Gao, W.; Su, R.; Li, N.; Gao, Y.; Xie, Y.; Kong, F.; Tang, B. A near-infrared reversible fluorescent probe for real-time imaging of redox status changes in vivo. *Chem. Sci.* **2013**, *4*, 1079−1086.
(39) Press, D. J.; Back, T. G. Enhanced gutathione peroxidase activity of conformationally restricted naphthalene peri-dichalcogenides. *Org. Lett.* **2011**, *13*, 4104−4107.
(40) Doğan, E. E. Hydrogen production and its storage from solar energy. *Adv. Mater. Sci.* **2020**, *20*, 14−25.
(41) Ji, S.; Xia, J.; Xu, H. Dynamic chemistry of selenium: Se-N and Se-Se dynamic covalent bonds in polymeric systems. *ACS Macro Lett.* **2016**, *5*, 78−82.
(42) (a) Wang, B.; Li, P.; Yu, F.; Song, P.; Sun, X.; Yang, S.; Lou, Z.; Han, K. A reversible fluorescence probe based on Se−BODIPY for the redox cycle between HClO oxidative stress and H_2S repair in living cells. *Chem. Commun.* **2013**, *49*, 1014−1016. (b) Manjare, S. T.; Kim, S.; Heo, W. D.; Churchill, D. G. Selective and sensitive superoxide detection with a new diselenide-based molecular probe in living breast cancer cells. *Org. Lett.* **2014**, *16*, 410−412.
(43) Dolomanov, O. V.; Bourhis, L. J.; Gildea, R. J.; Howard, J. A. K.; Puschmann, H. OLEX2: a complete structure solution, refinement and analysis program. *J. Appl. Crystallogr.* **2009**, *42*, 339−341.
(44) Sheldrick, G. M. Crystal structure refinement with SHELXL. *Acta Crystallogr.* **2015**, *71*, 3−8.
(45) Frisch, M. J.; Trucks, G. W.; Schlegel, H. B.; Scuseria, G. E.; Robb, M. A.; Cheeseman, J. R.; Scalmani, G.; Barone, V.; Mennucci, B.; Petersson, G. A.; Nakatsuji, H.; Caricato, M.; Li, X.; Hratchian, H. P.; Izmaylov, A. F.; Bloino, J.; Zheng, G.; Sonnenberg, J. L.; Hada, M.; Ehara, M.; Toyota, K.; Fukuda, R.; Hasegawa, J.; Ishida, M.; Nakajima, T.; Honda, Y.; Kitao, O.; Nakai, H.; Vreven, T.; Montgomery, J. A., Jr.; Peralta, J. E.; Ogliaro, F.; Bearpark, M.; Heyd, J. J.; Brothers, E.; Kudin, K. N.; Staroverov, V. N.; Keith, T.; Kobayashi, R.; Normand, J.; Raghavachari, K.; Rendell, A.; Burant, J. C.; Iyengar, S. S.; Tomasi, J.; Cossi, M.; Rega, N.; Millam, J. M.; Klene, M.; Knox, J. E.; Cross, J. B.; Bakken, V.; Adamo, C.; Jaramillo, J.; Gomperts, R.; Stratmann, R. E.; Yazyev, O.; Austin, A. J.; Cammi, R.; Pomelli, C.; Ochterski, J. W.; Martin, R. L.; Morokuma, K.; Zakrzewski, V. G.; Voth, G. A.; Salvador, P.; Dannenberg, J. J.; Dapprich, S.; Daniels, A. D.; Farkas, O.; Foresman, J. B.; Ortiz, J. V.; Cioslowski, J.; Fox, D. J. *Gaussian 09*, Revision D.01; Gaussian, Inc.: Wallingford, CT, 2013.
(46) (a) Lee, C.; Yang, W.; Parr, R. G. Development of the Colle-Salvetti correlation-energy formula into a functional of the electron density. *Phys. Rev. B* **1988**, *37*, 785−789. (b) Becke, A. D. Density-functional thermochemistry. I. The effect of the exchange-only gradient correction. *J. Chem. Phys.* **1993**, *98*, 5648−5652.
(47) (a) Reed, A. E.; Curtiss, L. A.; Weinhold, F. Intermolecular interactions from a natural bond orbital, donor-acceptor viewpoint. *Chem. Rev.* **1988**, *88*, 899−926. (b) Glendening, E. D.; Badenhoop, J. K.; Reed, A. E.; Carpenter, J. E.; Bohmann, J. A.; Morales, C. M.; Landis, C. R.; Weinhold, F. *Natural Bond Orbital (NBO)*, Version 6.0; Theoretical Chemistry Institute: Madison, WI, 2013.

https://doi.org/10.1021/acsomega.4c05366
ACS Omega 2025, 10, 6396−6405